Constraints on Black Hole Jet Models Used As Diagnostic Tools of Event Horizon Telescope Observations of M87

Brian Punsly[1,2,3]
[1] 1415 Granvia Altamira, Palos Verdes Estates, CA 90274, USA; brian.punsly@cox.net
[2] ICRANet, Piazza della Repubblica 10 Pescara I-65100, Italy
[3] ICRA, Physics Department, University La Sapienza, Roma, Italy

Abstract

Jet models of Event Horizon Telescope (EHT) data should also conform to the observed jet profiles just downstream. This study evaluates conformance of models of black hole (BH) jets to images of the innermost jet of M87. This is a basic test that should be passed before using them to perform a physical interpretation of EHT data. Recent 86 GHz very long baseline interferometry observations of M87 have revealed the morphology and size of the jet near its source ($<65\,M$, or 0.06 lt-yr after correcting for the line of sight to the jet, where M is the BH mass in geometrized units) for the first time. Current transverse resolution indicates that this region is dominated by flux emanating from the edge of the jet. The observed inner jet profiles are compared to all existing published synthetic radio images constructed from "state of the art" 3D numerical simulations of the BH accretion system in M87. Despite efforts to produce the characteristic wide, edge-dominated jet, these models are too narrow (by a factor of $\sim$2) in the region 0.06–0.32 lt-yr from the source, even though the jets (spine and/or sheath) in the image plane might appear conformant farther downstream. Furthermore, the synthetic radio images are not edge dominated 0.06–0.32 lt-yr from the source, but spine dominated. Analyses that implement these models as physical diagnostics of EHT visibility amplitudes are therefore suspect. Thus, these inner-jet characteristics are important considerations before applying simulations to the EHT data.

Key words: black hole physics – galaxies: active – galaxies: jets

1. Introduction

The study of relativistic jets from active galactic nuclei depends on the imaging provided by large-scale radio and microwave interferometers. These instruments provide the only high-resolution images. Most of our theories and insight have been based on early images from 25 to 40 yr ago. These observations image the jet very far from the source in terms of a scale set by the size of the central supermassive black hole (BH). Namely, if the mass of the central BH is M in geometrized units, then these "high-resolution" observations were defining features $10^3 M$–$10^6 M$ from the central BH. One of the great advances in modern astronomy is the improvement in resolution of these interferometers in the past decade. In particular, millimeter-band very long baseline interferometry (VLBI) routinely produces quality images at 7 mm. However, it is the recent ability to produce robust images at 3 mm that has finally resolved the region $\sim$60–350 M from the central BH in M87, after line of sight (LOS) de-projection (distances are de-projected unless otherwise stated). Thus, we are finally detecting size and morphology that can be reliably related directly back to the source itself as opposed to the huge extrapolations from light years away. The next decade promises refinement of these images with the addition of more baselines to the VLBI network with the ultimate goal of producing quality images at 0.8 and 1.3 mm with the Event Horizon Telescope (EHT). The physical interpretation of the EHT images will depend on the suite of numerical models that they are tested against. This study takes the first critical look at whether the models that we currently have are suitably conformant to the existing data $\sim$60–350 M from the central BH to justify extrapolation back to the EHT emission region. This is not a minor detail of the theory, this is the region that has the strongest direct causal connection to the jet-launching mechanism.

In spite of the early stages of these observations, the 86 GHz VLBI observations have already provided robust results that could not have been expected from simple jet models extrapolated toward the source from $10^3 M$–$10^6 M$ away. The nearby, $<350\,M$, size and morphology is directly compared with computations produced from existing theories and numerical models of BH jets for the first time. Previous treatments have stressed conformance to larger scales, without rigorous quantitative analysis at small distance near the jet source, which is the region of primary interest.

It is not trivial to compare the profile indicated by 86 GHz VLBI observations of the inner jet of M87 to existing theory and models of BH-driven jets. The jet boundary in simulations has various definitions (Dexter et al. 2012; McKinney et al. 2012; Sadowski et al. 2013). A particular notion of jet "width" is undefined in the image plane and cannot be compared to observation without an emissivity profile convolved with the restoring beam of comparison radio images. The vast majority of simulations in the literature are lacking in this regard. Fortunately, there are two numerical studies that have produced synthetic radio images of their numerical models, so that a direct comparison with the VLBI data is now possible (Mościbrodzka et al. 2016; Chael et al. 2019). The LOS that is used to project these models onto the sky plane is crucial. The 86 GHz VLBI data of Kim et al. (2018) is processed assuming a LOS of 18°, while the models of Mościbrodzka et al. (2016) and Chael et al. (2019) assume 20° and 17°, respectively. In this analysis we assume a range of LOS, 17°–25° (Stawarz et al. 2006; Mertens et al. 2016). Furthermore, it is assumed that the mass of central BH is $M_{\rm bh} \approx 6 \times 10^9 M_\odot$ or $M \approx 8.86 \times 10^{14}$ cm in geometrized units, which equates to

$\approx 3.5\mu$as at 16.7 Mpc (Gebhardt et al. 2011). Section 2 will describe the inner jet profile as given by the 86 GHz VLBI observations. Section 3 compares and contrasts VLBI images with numerical models.

2. The Innermost Profile of the Jet of M87

M87 has been monitored with the Very Long Baseline Array (VLBA) at 43 GHz since the beginning of the century (Walker et al. 2016). This has provided detailed information on scales larger than 0.3 mas. In this Letter, longer baseline data from the Global mm-VLBI Array (GMVA) at 86 GHz is used to study the jet structure on smaller scales, 0.05–0.35 mas (Kim et al. 2018).

The top frame of Figure 1 shows the jet width as derived by Kim et al. (2018) from the GVMA observations that they studied. These data are extracted from the stacking of five observations spread out from 2004 to 2015 and was presented in their Figure 6. The analysis is facilitated by the existence of two pronounced ridges of emission that has been referred to as edge brightening. The jet width is the distance between the peak brightness of the ridges. The Kim et al. (2018) data in the plot extends 340 M from the jet source. The bottom frame changes the assumed LOS from 18° to 25°. These plots are restricted to a smaller distance from the source than was chosen in Kim et al. (2018) during their fitting process. By choosing many points farther from the BH, the fit to the jet in the vicinity of the source is not optimized because it is overwhelmed by weighting the least squares fit with residuals of the numerous points $\sim$1000 M from the source. Thus, most of the points that are displayed in Figure 1 are circumvented by their fit, which is dominated by points farther out. This might be justifiable if the one insisted on a single power-law fit over all distance scales. However, this is not directly motivated by the observational data itself, but by simple theoretical models (Blandford & Königl 1979). The Kim et al. (2018) power-law fit to the jet width, $W(z)$, as function of axial displacement along the jet, z, is $W(z) \propto z^{-k}$, $k = 0.498 \pm 0.025$. This study is an attempt to be a bit more rigorous. A uniform power law over the innermost few light years of jet propagation is not assumed in the following. The data is restricted to a range of 3.8 light months ($z < 340M$, $100M \approx 0.0937$ lt-yr). There are certainly ample data in this regime and it is far from the source in terms of the FWHM of the circular Gaussian fit to the EHT emission at 230 GHz ($\sim$40 μas) shown schematically near the left edge of both panels of Figure 1 (Doeleman et al. 2012; Akiyama et al. 2015). Second, the uncertainty in the data is considered in the fit to $W(z)$. The uncertainty in z is half the distance between the points in Figure 6 of Kim et al. (2018) and the error in $W(z)$ is from Figure 6 of that paper. The method of Reed (1989) is used to fit the data with uncertainty in both variables. The power-law index is $k = 0.230 \pm 0.049$. The Kim et al. (2018) data is validated by the close alignment of the 2014 VLBI data of Hada et al. (2016) in Figure 1. The dashed lines in Figure 1 indicate the standard error of the Reed (1989) fit to the data. Note that the synchrotron self-absorption core shift at 86 GHz is assumed to be 10.5 μas based on the analysis of Hada et al. (2011). The fits are insensitive to the uncertainty in the small core offset, so it is not critical to know this value exactly.

The fit in Figure 1 has two interesting implications. First, the jet within 3.8 light months from the source is much more collimated than a parabolic jet, $k = 0.5$. Second, if one extrapolates to within $\sim$20M of the central BH, we see that

the jet is $\sim$2–3 wider than the size of the circular Gaussian fit to the correlated EHT flux. Thus, this extrapolation is not justified. The jet must have a very large opening angle at small z in order for the EHT data to join with the power-law fit to the GMVA data 0.7–3.8 light months of the source. The maximum z at which this large opening can collimate is the innermost GVMA data point. This results in the minimum possible intrinsic opening angle of the jet base, $>65°$, where the fitted power law was chosen to represent the innermost data point. It is larger if we use the data point itself, extrapolate the fit closer to the BH, or assume an LOS $> 18°$.

3. Comparison of the Inner Jet Profile of M87 with Models of BH Jets

Only 3D models of radiatively inefficient BH accretion are considered relevant for M87 (Narayan & Yi 1994). The nexus to VLBI observation requires a synthetic image to be made from the simulation with the same restoring beam (same resolution limits) as the comparison radio image. Currently, there are only two numerical studies for which such images have been generated by the researchers. The magnetic flux in the central funnel of the accretion disk ranges from modest to large, SANE and MAD (magnetically arrested), respectively (Igumenshchev et al. 2003; Tchekhovskoy et al. 2011; Narayan et al. 2012). The SANE simulation radiates entirely from a funnel wall jet (FWJ) at the funnel/disk interface (Mościbrodzka et al. 2016). The MAD simulations in Chael et al. (2019) have been argued to be required to power the jet in M87. They radiate from the FWJ and, to some degree, the adjacent regions of the interior jet. Both models assume rapidly rotating BHs, $a/M = 0.9375$, where a is the angular momentum per unit mass of the BH.

3.1. FWJs

In Figure 6 of Mościbrodzka et al. (2016), the simulated emissivity is restored with the same beam as the stacked 43 GHz VLBI observations of Hada et al. (2013), 0.30 mas × 0.14 mas that is shown in the top frame of Figure 2. Figure 2 provides some metrics to quantify the jet profiles within the context of the radio (real and synthetic) images. Fortunately, there are contour levels in their Figure 6 that can be used to evaluate the observed surface brightness distribution, $S(\rho, z)$. The axial displacement along the red jet center line 0.2–0.4 mas from the radio core, z, and transverse displacement, ρ, as projected on the sky plane are illustrated in the top frame. Using this coordinate system, Figure 2 explores the axial surface brightness, $S^A(z) \equiv S(\rho = 0, z)/S(\rho = 0, z = 0)$ and the jet 0.5 contour or half width,

$$S_{0.5}(z) = \rho_{+0.5}(z) - \rho_{-0.5}(z),$$
$$S[\rho = \rho_{+0.5}(z), z]\Theta(\rho) \equiv 0.5S(\rho = 0, z),$$
$$\text{and } S[\rho = \rho_{-0.5}(z), z]\Theta(-\rho) \equiv 0.5S(\rho = 0, z), \quad (1)$$

where Θ is the Heaviside step function. One can determine $S^A(z)$ and $S_{0.5}(z)$ everywhere the center line crosses one of the plotted surface brightness contours. The contour levels have a ratio of $\sqrt{2}$. The top frame of Figure 2 displays the evaluation of $S_{0.5}(z)$ at $z = 0.26$ mas by the length of the blue segment orthogonal to the center line. The bottom frame of Figure 2 shows that $S^A(z)$ in the model decays slightly slower than the radio image as z increases. Yet, $S(\rho, z = \text{contant})$ decays
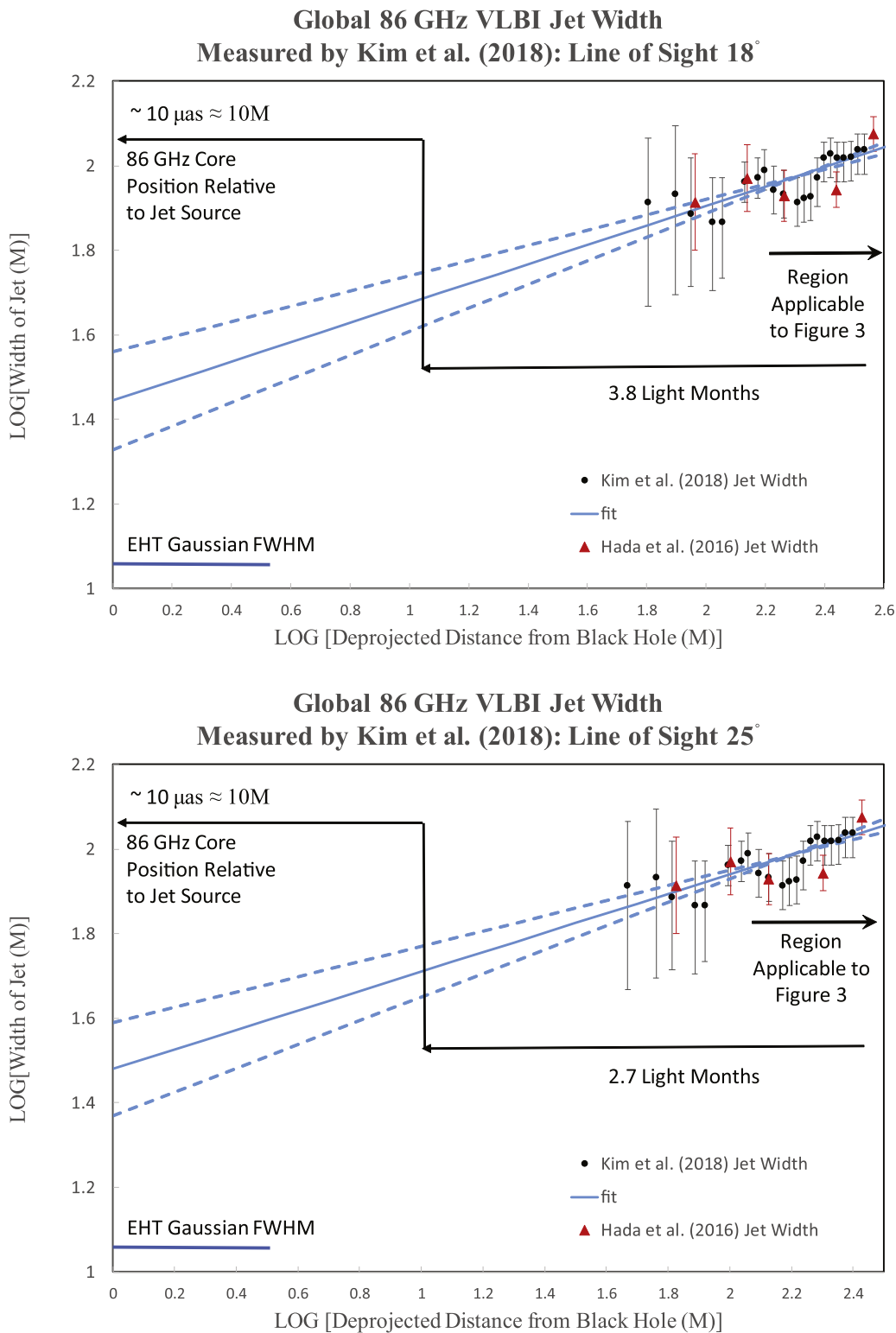
Global 86 GHz VLBI Jet Width
Measured by Kim et al. (2018): Line of Sight 18°

Global 86 GHz VLBI Jet Width
Measured by Kim et al. (2018): Line of Sight 25°

Figure 1. The top panel shows the fit with uncertainty in both variables to the M87 86 GHz VLBI jet width profile. The data is from of Kim et al. (2018) who assumed an LOS of 18°. The fitted data extends ~3.8 light months from the unresolved radio core. The bottom panel is the fit assuming an LOS of 25°. The power-law index is unchanged, but the width extrapolates to be wider at $z = 0$. The location of the EHT correlated flux is not known, but it is shown schematically in the lower left-hand corner.

much more rapidly with ρ in the model than the radio image. In order compute the uncertainty of the $S_{0.5}(z)$ estimate, note that the monotonic increase in $S_{0.5}(z)$ tracks the increase in the double ridge line estimate of $W(z)$ in Figure 3 of Hada et al. (2013) with a positive offset ≈ 0.2 mas. Thus, the systematic

uncertainty of the $S_{0.5}(z)$ estimate, σ_s, is identified with the uncertainty of $W(z)$ in Hada et al. (2013), Figure 3, as 12%. The uncertainty in the contour intensity level from thermal noise is chosen as 3 rms = 3.9 mJy/beam. This induces an uncertainty in the position of the contour level in the image plane. For
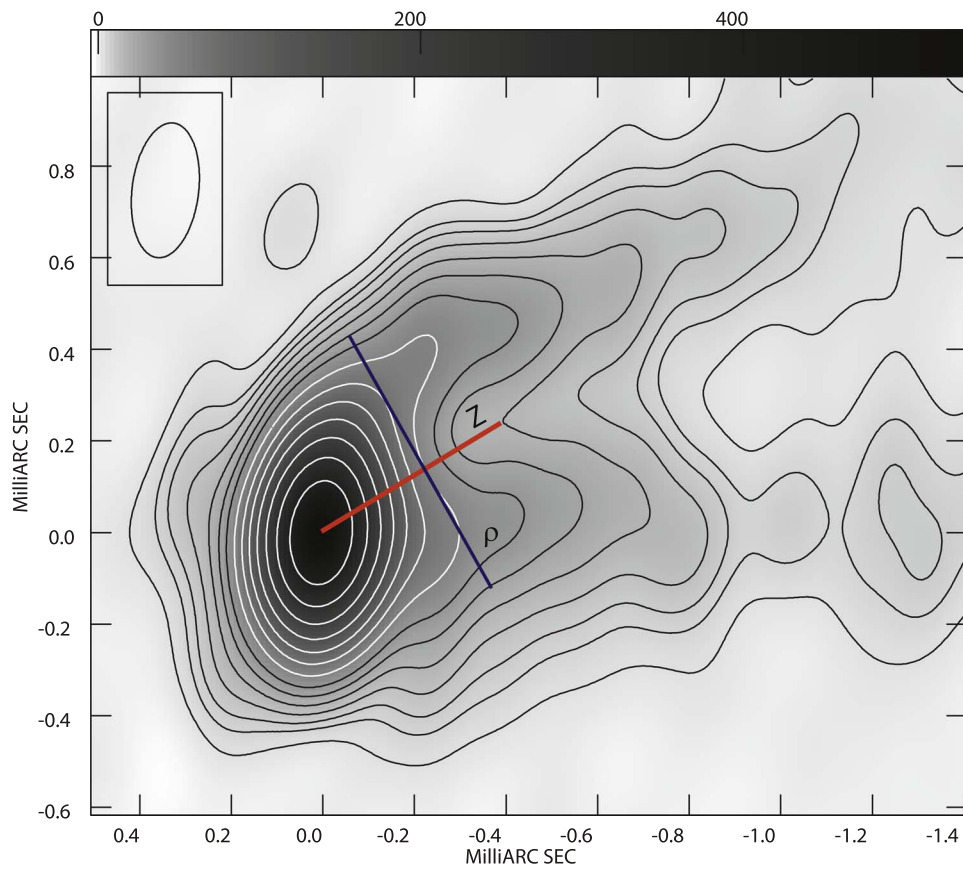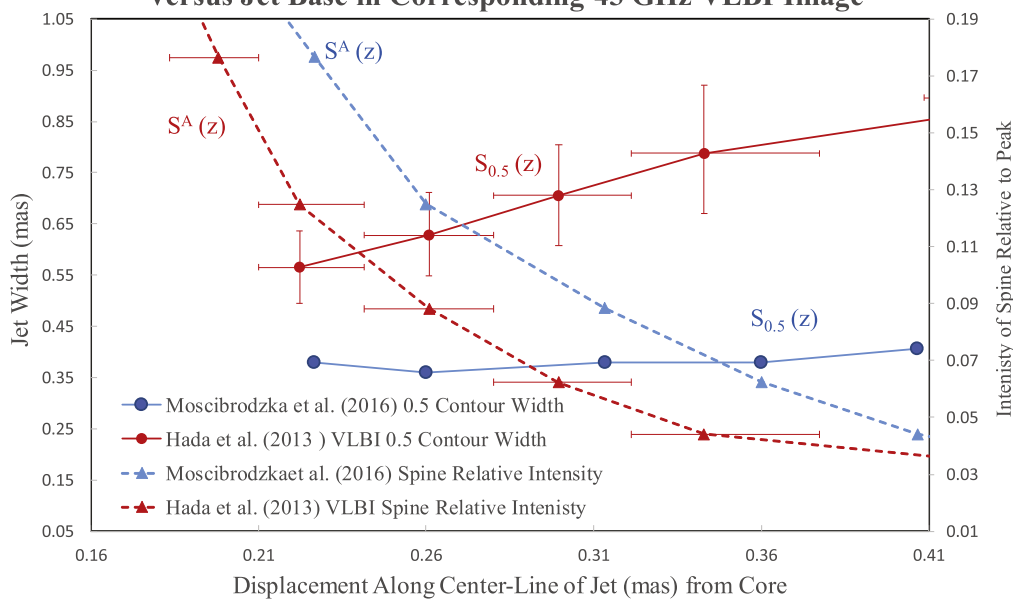
Figure 2. The top frame shows the 43 GHz VLBA image provided by K. Hada that is used for comparison with the FWJ model. The blue ρ-axis crosses the red z-axis at $z = 0.26$ mas. The contours are $\sqrt{2}$ increments. The length of the blue segment indicates that $S_{0.5}(z = 0.26 \text{ mas}) = 0.63$ mas. The bottom frame compares the FWJ model surface brightness with the image after restoration with the same beam. The lines between points do not represent intermediate values, but merely draw one's eye to the overall trend.

example, if the intensity level is increased by 10%, as the contour levels are every factor of 1.41, then this increase induces a shift of approximately 0.1/0.41 toward the adjacent

contour level along the blue line in the top frame of Figure 2. This shift of the intensity contour due to thermal noise is the uncertainty, σ_t. The resultant uncertainty of $S_{0.5}(z)$ is
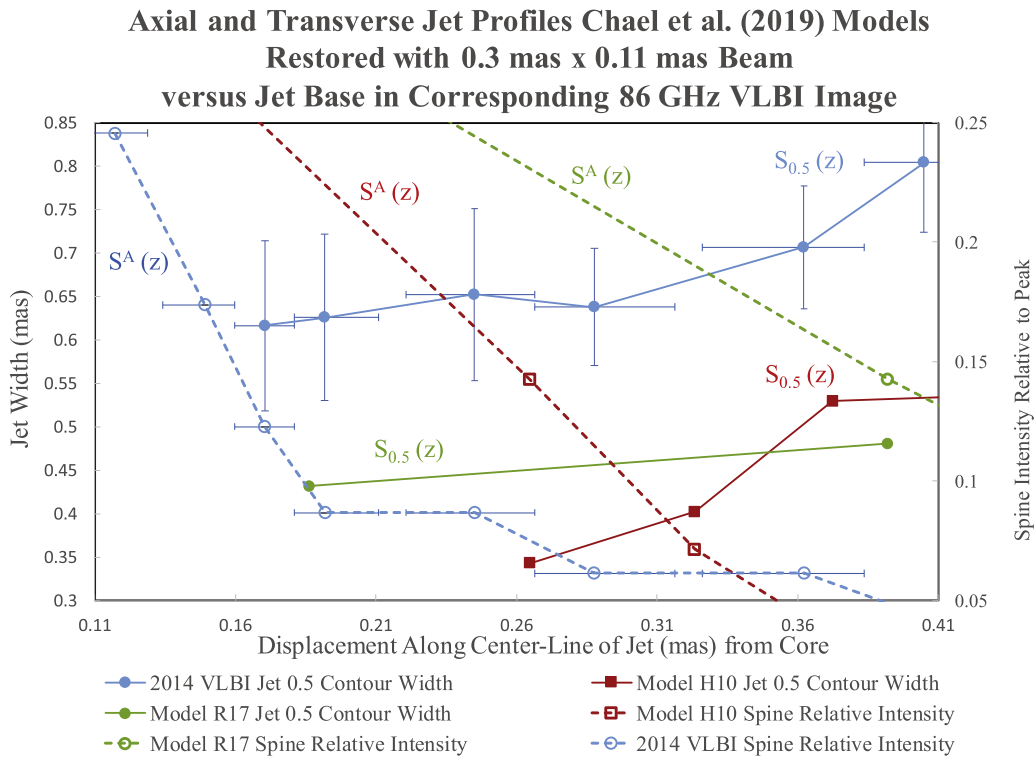
Figure 3. The top frame compares the inner jet profile of the Hada et al. (2016) 86 GHz observation with the two models H10 and R17 of Chael et al. (2019) after restoration with the same beam. The bottom frame is the same at 43 GHz. See the text for details.

$\sigma = \sqrt{\sigma_s^2 + \sigma_t^2}$. The axial positional uncertainty is 1%–10% in Hada et al. (2013). This motivates the conservative choice of uncertainty, which is the smaller of half the distance to the adjacent contour and $0.1z$.

Even though the intrinsic emissivity distribution in Mościbrodzka et al. (2016) is approximately a δ-function at the maximum value of ρ at each z, the image appears spine dominated and not edge dominated because of the "large" 0.3 mas beamwidth in the transverse direction. By contrast, the VLBI image is not spine dominated, but edge dominated for $z > 0.25$ mas. Thus, these FWJ simulations do not represent the M87 jet near its source.

It is of interest to quantify the intrinsic difference between the width of the inner jet of M87 and the width of the FWJ. This is possible due to the fact that the luminosity distribution is restricted to a very thin boundary layer in both M87 and the model. At 0.2 mas from the source, it was shown in Figure 5 of Punsly et al. (2018) that the *intrinsic* surface brightness associated with the 86 GHz VLBI observation of Hada et al. (2016) is approximately a double δ-function, $S_{\rm int}(\rho, z = 0.2 \, {\rm mas}) \approx S_{\rm Hada}[0.48\delta(\rho + 0.15 \, {\rm mas}) + \delta(\rho - 0.15 \, {\rm mas})]$, where $S_{\rm Hada} = 19$ mJy/beam is a normalization constant. The observed $S(\rho, z = 0.2 \, {\rm mas})$ restored with the full beam is highly blurred, but still edge dominated (Hada et al. 2016). Similarly, from Figure 4 of Mościbrodzka et al. (2016), $S_{\rm int}(\rho, z = 0.2 \, {\rm mas}) \approx S_-\delta(\rho + 0.075 \, {\rm mas}) + S_+\delta(\rho - 0.075 \, {\rm mas})$, where S_+ and S_- are constants that cannot be determined from the article. The blurring of the surface brightness by the VLBI restoring beam reduces the ratio of the 0.5 contour widths in the bottom frame of Figure 2 relative to the intrinsic ratio of the physical dimensions, given by $\approx [2(0.15 \, {\rm mas})]/[2(0.075 \, {\rm mas})] = 0.3 \, {\rm mas}/ 0.15 \, {\rm mas} = 2$.

3.2. MAD Models

Figure 3 compares the width of the inner jet, as determined from observation, with numerical models in Chael et al. (2019), H10 and R17. The simulations of Chael et al. (2019) match the $55°$ opening angle in the image plane gleaned from 43 GHz VLBA (Walker et al. 2018). But this agreement with the jet occurs at $z = 0.5\text{--}1.9$ mas. By contrast, Figure 3 considers $z < 0.4$ mas (recall the different value of k found by Kim et al. 2018 by considering more distant points than are chosen in Figures 1). Figures 10 and 11 of Chael et al. (2019) are an effort to directly compare the simulations to VLBI images at 43 GHz and 86 GHz, respectively. The authors have processed the observational data and the numerical results with the same restoring beam. In spite of this, the comparison is not trivial because the jet morphology is different between the models and the observations within 0.4 mas. The flux from the M87 jet is dominated by the edges on these small scales (see Figure 5 of Punsly et al. 2018), but the images produced by the simulation have jets in which the flux is concentrated along the axis of the jet. One might say that the M87 jet is extremely edge brightened for $z < 0.4$ mas, and the H10 and R17 simulations are edge darkened for $z < 0.4$ mas.

The top frame of Figure 3 applies the metrics used to describe $S(\rho, z)$ for the FWJ, to the 86 GHz image and models presented in (Chael et al. 2019). Because the 86 GHz image was originally restored in Hada et al. (2016) with a similar beam, the original image was used as it is has higher contour resolution (every $\sqrt{2}$ instead of 2). Figure 9 and Table 1 of Hada et al. (2016) provide the data for σ_s and σ_t, respectively, that are used in computing the errors (as in Figure 2) in the top frame of Figure 3; see also the demarcated region in the top right-hand corner of Figure 1. At 43 GHz, in the bottom frame, the contour levels in Chael et al. (2019) are at 47% not 50% (the contour decrement is 2.15 not 2), so one must use 0.47 instead of 0.5 in Equation (1). The same parameters are used to compute the uncertainty in the bottom frame as were used in Figure 2. At both frequencies $S(\rho, z = {\rm contant})$ decays much more rapidly with ρ in the models compared to the observation, and $S^A(z)$ decays much more slowly with z in the models compared to the observations. The Chael et al. (2019) simulations are much narrower than the observed jet in M87

at 43 and 86 GHz for $z < 0.4$ mas. Furthermore, the spine is too pronounced, and M87 is very edge dominated at 86 GHz for $z < 0.4$ mas. Figure 3 indicates that these MAD simulations do not represent the M87 jet accurately near its source.

4. Conclusion

This study proposes guidelines based on observation that models should follow before application to the EHT region of M87. Namely, the observed jet profile within 0.35 mas of the core in M87 is compared with jet profiles from models of BH-driven jets. In Section 2, it was shown that the jet base within 0.06 lt-yr of the source is widely flared with an intrinsic opening angle $>65°$, and the jet is highly collimated for 0.06 lt-yr $< z <$ 0.32 lt-yr. In Section 3, it was demonstrated that all published synthetic radio images from BH jet models produce jets that are too narrow relative to M87 on scales 0.06 lt-yr $< z <$ 0.32 lt-yr. The synthetic images are not edge dominated, like the images of M87, but spine dominated for 0.06 lt-yr $< z <$ 0.32 lt-yr. These are not minor discrepancies of the theory, this is the region that has the strongest direct causal connection to the jet-launching mechanism.

Three models were analyzed with different electron temp-erature prescriptions (although all produce a funnel and funnel wall that is hotter than the disk) and different funnel magnetic field strengths. All showed a similar discrepancy in the axial and transverse intensity. The discrepancy that was found is not an issue of time variability, it occurred with different telescopes and different frequencies over a ~ 10 yr period ($t > 10^4 M$). Model parameters such as the treatment of the polar axis, disk size and tilt, funnel magnetization, and the jet-launching region can affect the jet width (Dibi et al. 2012; Sadowski et al. 2013; Punsly 2017). It is not clear, nor claimed, that Figures 2 and 3 capture the widest, most edge-dominated possible simulated jets for $z < 0.35$ mas. It is difficult to assess the simulations without synthetic images. However, a $\pm 20\%$ variation in SANE jet width at $z = 50M$ in code validation studies with convergent numerical resolution is noted (Porth et al. 2019). A $\pm 20\%$ uncertainty, after beam convolution, will not alter the results of Figure 2. There is no such study for MAD jets (Porth et al. 2019). MAD jets spread to wider opening angles due to enhanced internal magnetic pressure. The horizon magnetiza-tion, normalized to the accretion rate, is defined in Chael et al. (2019), $\phi_{\rm BH} = 55\text{--}63$. These simulations are at or near full magnetic flux saturation in the funnel (Tchekhovskoy 2015). Therefore, these jets might attain near maximal MAD jet width. More simulated synthetic images are required to explore the generality of these results and the physical assumptions that ameliorate these discrepancies.Acknowledgments

ORCID iDs

Brian Punsly ⓘ https://orcid.org/0000-0002-9448-2527

References

Akiyama, K., Lu, R., Fish, V., et al. 2015, ApJ, 807, 150
Blandford, R., & Königl, A. 1979, ApJ, 232, 34
Chael, A., Narayan, R., & Johnson, M. D. 2019, MNRAS, 486, 2873
Dexter, J., McKinney, J. C., & Agol, E. 2012, MNRAS, 421, 151
Dibi, S., Drappeau, S., Fragile, P. C., Markoff, S., & Dexter, J. 2012, MNRAS, 426, 1928
Doeleman, S., Fish, V., Schenck, D., et al. 2012, Sci, 338, 355
Gebhardt, K., Adams, J., Richstone, D., Lauer, T. R., & Faber, S. M. 2011, ApJ, 729, 119
Hada, K., Doi, A., Kino, M., et al. 2011, Natur, 477, 185
Hada, K., Kino, M., Doi, A., et al. 2013, ApJ, 775, 70
Hada, K., Kino, M., Doi, A., et al. 2016, ApJ, 817, 131
Igumenshchev, I. V., Narayan, R., & Abramowicz, M. A. 2003, ApJ, 592, 1042
Kim, J.-Y., Krichbaum, T., Lu, R.-S., et al. 2018, A&A, 616, A188
McKinney, J., Tchekhovskoy, A., & Blandford, R. 2012, MNRAS, 423, 3083
Mertens, F., Lobanov, A., Walker, R., & Hardee, P. 2016, A&A, 595, 54
Mościbrodzka, M., Falcke, H., & Shiokawa, H. 2016, A&A, 586, 38
Narayan, R., Sadowski, A., Penna, R. F., & Kulkarni, A. K. 2012, MNRAS, 426, 3241
Narayan, R., & Yi, I. 1994, ApJL, 428, 13
Porth, O., Chaterjee, K., Narayan, R., et al. 2019, arXiv:1904.04923v1
Punsly, B. 2017, ApJ, 850, 190
Punsly, B., Hardcastle, M., & Hada, K. 2018, A&A, 614, 104
Reed, B. 1989, AmJPh, 57, 642
Sadowski, A., Narayan, R., Penna, R. F., & Zhu, Y. 2013, MNRAS, 436, 3856
Stawarz, L., Aharonian, J., Kataoka, J., et al. 2006, MNRAS, 370, 981
Tchekhovskoy, A. 2015, The Formation and Disruption of Black Hole Jets, Astrophysics and Space Science Library, Vol. 414 (Switzerland: Springer International Publishing)
Tchekhovskoy, A., Narayan, R., & McKinney, J. C. 2011, MNRAS, 418, L79
Walker, R. C., Hardee, P. E., Davies, F., et al. 2016, Galax, 4, 46
Walker, R. C., Hardee, P. E., Davies, F. B., Ly, C., & Junor, W. 2018, ApJ, 855, 128